Dedicated to innovation in aerospace

NLR-TP-2016-002 | March 2018

Single scan vector prediction in selective laser melting

CUSTOMER: Ministry of Economic Affairs

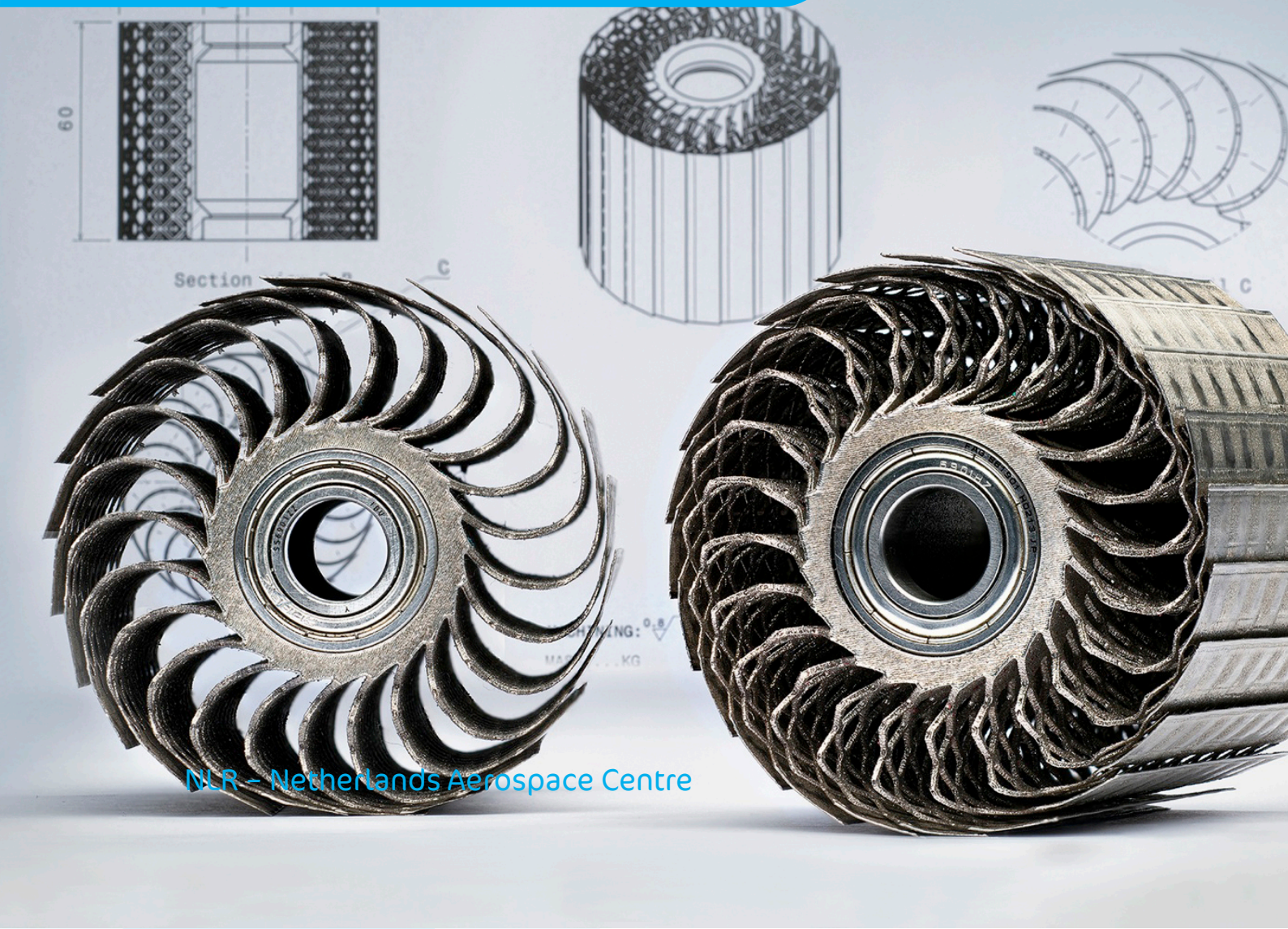

NLR – Netherlands Aerospace Centre

Netherlands Aerospace Centre

NLR is a leading international research centre for aerospace. Bolstered by its multidisciplinary expertise and unrivalled research facilities, NLR provides innovative and integral solutions for the complex challenges in the aerospace sector.

NLR's activities span the full spectrum of Research Development Test & Evaluation (RDT & E). Given the NLR's specialist knowledge and facilities, companies turn to the NLR for validation, verification, qualification, simulation and evaluation. The NLR thereby bridges the gap between research and practical applications, while working for both government and industry at home and abroad.
NLR stands for practical and innovative solutions, technical expertise and a long-term design vision. This allows the NLR's cutting edge technology to find its way into successful aerospace programs of OEMs, including Airbus, Embraer and Pilatus. NLR contributes to (military) programs, such as ESA's IXV re-entry vehicle, the F-35, the Apache helicopter, and European programs, including SESAR and Clean Sky 2.
Founded in 1919, and employing some 650 people, the NLR achieved a turnover of 73 million euros in 2014, of which three-quarters derived from contract research, and the remaining from government funds.

For more information visit: **www.nlr.nl**

Dedicated to innovation in aerospace

Single scan vector prediction in selective laser melting

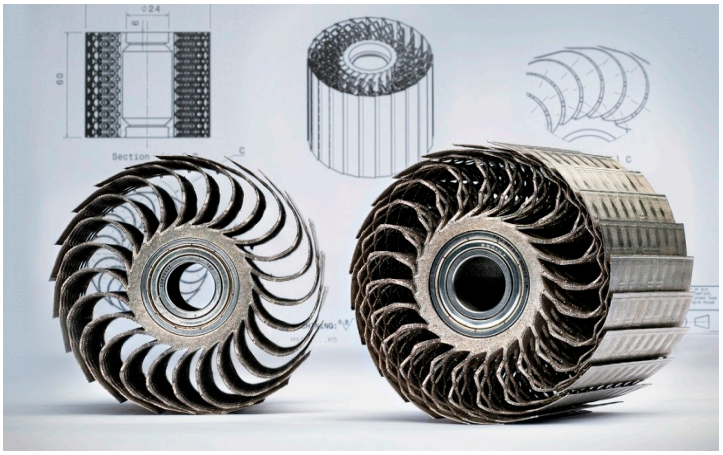

Problem area

In selective laser melting (SLM) products are built by melting layers of metal powder successively. Optimal process parameters are usually obtained by scanning single vectors and subsequently determining which settings lead to a good compromise between product density and build speed.

Description of work

A model was developed that describes the effects occurring when scanning single vectors. Energy absorption and heat conduction are modeled to determine the temperature distribution and melt pool characteristics for different laser powers, scan speeds and layer thicknesses.

REPORT NUMBER
NLR-TP-2016-002

AUTHOR(S)
W.W. Wits
R. Bruins
L. Terpstra
R.A. Huls
H.J.M. Geijselaers

REPORT CLASSIFICATION
UNCLASSIFIED

DATE
March 2018

KNOWLEDGE AREA(S)
Gasturbine Technology
Computational Mechanics and Simulation Technology
Structures and Manufacturing Technology

DESCRIPTOR(S)
SLM

Results and conclusions

The model shows good agreement with experimentally obtained scan vectors widths.

Applicability

The mode can be used to predict SLM process parameters for a given powder. It can also give insight in the temperature development on the melt pool scale, which can input for a deformation prediction for production of an entire product.

GENERAL NOTE
This report is based on an article published in Additive Manufacturing 9, 2016, by Elsevier.

NLR
Anthony Fokkerweg 2
1059 CM Amsterdam
p) +31 88 511 3113 f) +31 88 511 3210
e) info@nlr.nl i) www.nlr.nl

Dedicated to innovation in aerospace

NLR-TP-2016-002 | March 2018

Single scan vector prediction in selective laser melting

CUSTOMER: Ministry of Economic Affairs

AUTHOR(S):

W.W. Wits	University of Twente
R. Bruins	Nationaal Lucht- en Ruimtevaartlaboratorium
L. Terpstra	University of Twente
R.A. Huls	Nationaal Lucht- en Ruimtevaartlaboratorium
H.J.M. Geijselaers	University of Twente

NLR - Netherlands Aerospace Centre

This report is based on an article published in Additive Manufacturing 9, 2016, by Elsevier.

CUSTOMER	**Ministry of Economic Affairs**
CONTRACT NUMBER	**------**
OWNER	**NLR**
DIVISION NLR	**Aerospace Vehicles**
DISTRIBUTION	**Unlimited**
CLASSIFICATION OF TITLE	**UNCLASSIFIED**

APPROVED BY :		
AUTHOR	**REVIEWER**	**MANAGING DEPARTMENT**
R.A. Huls	G. van de Vrie	O.S. Zoeteweij
DATE 29 03 18	DATE 29 03 18	DATE 06 04 18

Summary

In Selective Laser Melting (SLM) products are built by melting layers of metal powder successively. Optimal process parameters are usually obtained by scanning single vectors and subsequently determining which settings lead to a good compromise between product density and build speed. This paper proposes a model that describes the effects occurring when scanning single vectors. Energy absorption and heat conduction are modeled to determine the temperature distribution and melt pool characteristics for different laser powers, scan speeds and layer thicknesses. The model shows good agreement with experimentally obtained scan vectors and can therefore be used to predict SLM process parameters.

Keywords: Additive manufacturing; Selective laser melting (SLM); Process control; Predictive modeling; Scan vector melting

This page is intentionally left blank.

Contents

This page is intentionally left blank.

1 Introduction

The Selective Laser Melting (SLM) process builds products by melting successive layers of metal powder and is therefore classified as an Additive Manufacturing (AM) process. SLM is forecasted to partially replace conventional manufacturing processes for high-tech engineered products with its capability to manufacture high-value, low-volume, (near) net-shape parts [1].

Two important challenges in SLM production are part distortion by thermal stresses, and obtaining good and reproducible part properties [2]. The main focus of this paper is on the latter. However, the results of this study will also be used as input for methods treating the former (residual stress prediction). The properties of SLM manufactured parts strongly depend on the quality of each single laser-melted track. Moreover, obtaining uniform tracks well attached to the substrate or previous layer is a necessary requirement for the fabrication of high-quality parts [3]. Kruth et al. [4] reported that for this a good compromise between wetting, remelting, solidification and powder bed characteristics is essential.

The SLM process is characterized by a large number of parameters such as laser power, scan speed, spot size, scan line spacing (hatch distance), thickness of the powder layer, scanning strategy, working atmosphere, temperature of powder bed, and material properties. All of these parameters have an effect on the track formation. Unfortunately, their mutual interaction is not always clear [5].

This paper addresses the prediction of single laser-melted tracks (i.e. the scan vector or straight line that the laser converts into a solid track) in order to find the optimal process settings. The quality of single tracks depends on a limited set of the aforementioned process parameters. The most important process parameters for the production of single tracks are the laser power, scan speed, laser spot size and the thickness of the deposited powder layer. Suitable ranges of process parameter values for optimal mechanical properties or minimal process time can be obtained experimentally by producing short tracks using many single scan vectors and examining the influence of each parameter change. This is however very time consuming and costly, especially considering the potential number of new materials and powders. Experimentation only also does not yield the necessary insights into the physical processes behind the results.

Therefore in this study a numerical model is developed and validated experimentally. The model can predict the resulting track width and attachment of single scan vectors based on the mentioned process parameters. The model improves process knowledge insight and reduces the cost of predicting parameter ranges for which single scan vectors are of good quality.

2 Numerical modeling

To predict the behavior of the laser melting and solidification of a single scan vector, this process is modeled in a finite element code. Due to the scan vector symmetry, a half symmetrical model is built (Figure 1). The metal powder bed is modeled as a homogenized powder layer on top of a solid substrate of the same material (i.e. the layer of material that was previously deposited). The length of the model in the direction in which the laser is moving is 2 mm, the thickness is 0.5 mm (5x the powder bed layer thickness) and the width is also 0.5 mm (approx. 14x the laser spot size radius), as shown in Figure 1. A track length of 1 mm is scanned. The dimensions are chosen such that a quasi-steady melt pool behavior is achieved for the parameter ranges of interest. Depositing multiple layers in the model is considered unnecessary, because scanning an entire layer in the experiments (described later) and then depositing a new powder layer takes sufficient time for the deposited layer to cool down to the preheat temperature.

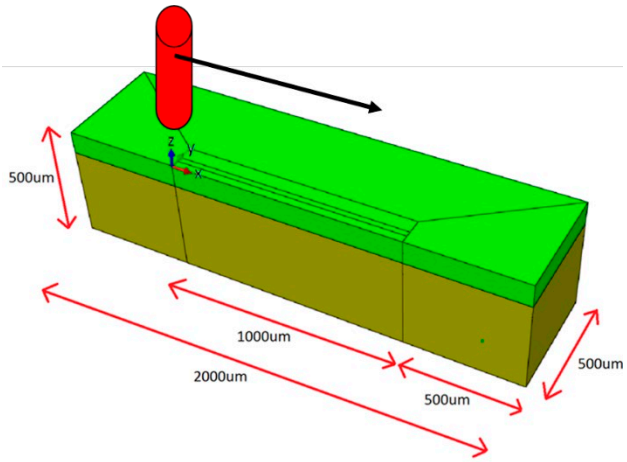

Figure 1. *Single scan vector model geometry (half symmetrical).*

The laser is modeled as a constant moving heat source using the Abaqus subroutine DFLUX. To minimize output fluctuations a minimum of four elements fit within the laser spot size. The numerical model is computed in Abaqus using an implicit backwards difference algorithm with a mesh of more than 10,000 nodes.
According to Gusarov [6] heat transfer by radiation and convection is small compared to heat transfer by conduction due to the large temperature gradients. Also in this study the radiative and convective heat losses at the surface were found to be irrelevant compared to the heat fluxes due to diffusion.
The initial preheating temperature is set to 453 K using a '*initial conditions' card. The temperature at the bottom interface of the model is kept constant at this temperature using a *boundary card to avoid heat accumulation. The boundary is located far enough from the melt pool to have a small influence on the temperature in the melt pool itself, which is the main interest of this paper. Thermal gradient driven mass flow in the melt pool is not considered in this work. Also, capillary instability of the melt pool is irrelevant for the selected process parameter ranges based on the Plateau-Rayleigh analysis [7].

2.1 Powder bed laser energy absorption

The laser energy absorption in the powder bed follows the description of Gusarov and Smurov [8] using slow consolidation, in which the powder bed is modeled as a packed bed of monodispersed opaque spheres. The powder bed acts as an optical medium for which the absorption of the laser energy is modeled using an effective extinction coefficient:

$$\beta = \frac{3(1-f)}{2fd_p} \tag{1}$$

Here, f is the powder bed porosity and d_p is the average powder particle diameter. The relative thickness of a powder bed with thickness z_{bed} is described by the optical layer thickness:

$$\tau_L = \beta z_{bed} \tag{2}$$

The powder bed absorbs part of the laser energy. The remainder is absorbed by the solid substrate underneath. The laser energy flux per unit area absorbed by the powder bed, where the powder and substrate are of the same material, can be expressed by [9]:

$$\frac{Q}{Q_0}(0) = \frac{\omega a}{(4\omega-3)D}\{2(1-\omega^2)e^{-\tau_L} - (3+\omega e^{-2\tau_L}) \times (p_1+p_2)\} - \frac{3(1-\omega)(1-\omega e^{-2\tau_L})}{4\omega-3} \tag{3}$$

In which:

$$a = \sqrt{1-\omega} \tag{4}$$

$$D = (1-a)p_2 - (1+a)p_1 \tag{5}$$

$$p_1 = [1+a-\omega(1-a)]e^{2a\tau_L} \tag{6}$$

$$p_2 = [1-a-\omega(1+a)]e^{-2a\tau_L} \tag{7}$$

Here, Q_0 is the uniform incident surface heat flux of the laser spot and ω is the reflectivity of the specular reflection. A significant part of the incident laser energy is absorbed by the powder layer. The remaining part of the laser energy that is absorbed by the solid substrate is described by:

$$\frac{Q}{Q_0}(\tau_L) = \frac{\omega a}{(4\omega-3)D}\{(1-\omega^2)e^{-\tau_L}[(1-a)e^{-2a\tau_L} + (1+a)e^{2a\tau_L}] - 2(1-\omega)(3+\omega e^{-2\tau_L})\} - \frac{3(1-\omega)(1-\omega)e^{-\tau_L}}{4\omega-3} \tag{8}$$

The energy absorption is modeled as a volumetric heat input applied to the volume underneath the laser spot. The properties of the powder are given in Table 1.

Table 1. *Powder bed properties relevant for the heat absorption.*

Property	***Symbol***	***Value***
Mean particle diameter	d_p	33 µm
Powder layer porosity	f	0.5
Reflectivity of the material	ω	0.64
Local powder layer thickness	z_{bed}	100 µm

To model the irradiated laser energy, a second order Gaussian beam shape profile is applied with a beam factor of two, associated with a laser intensity in the spot center of twice the average intensity. Figure 2 shows the penetration profile of the laser beam for a 200 W laser power and a laser spot size of 70 µm. The z-direction indicates the penetration depth, whereas the x-axis is the axial coordinate.

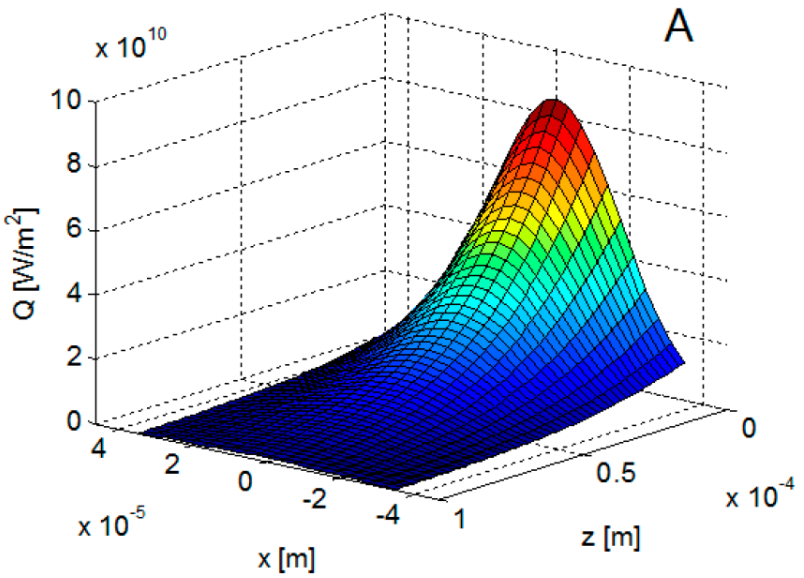

Figure 2. *Penetration profile of a 200 W laser beam and a laser spot size of 70 µm. The z-direction indicates penetration depth; the x-axis is the axial coordinate.*

2.2 Material properties

The material applied is titanium alloy Ti6Al4V. The material properties required are the thermal conductivity, heat capacity and density for both the substrate and the powder. The substrate properties were taken from Mills [10] and are listed in Table 2. For Ti6Al4V the transition from the solid (powder) phase to the liquid phase occurs between the solidus temperature (1878 K) and the liquidus temperature (1933 K). The boiling temperature is 3315 K.

Table 2. *Temperature dependent material properties for Ti6Al4V. Thermal conductivity k, specific heat capacity c_p, density ρ and latent heat of fusion Q_L. The first three rows are substrate properties; the next three rows are powder bed properties.*

Property	***Unit***	***293 K***	***1878 K***	***1933 K***	***3315 K***
k	$Wm^{-1}K^{-1}$	7	27.5	35	50
c_p	$Jkg^{-1}K^{-1}$	610	700	730	730
ρ	kgm^{-3}	4420	4200	3950	3780
k	$Wm^{-1}K^{-1}$	0.2	0.3	35	50
c_p	$Jkg^{-1}K^{-1}$	610	700	730	730
ρ	kgm^{-3}	2210	2100	1975	1890
Q_L	$kJkg^{-1}$		370		

The conductivity of the powder bed is mostly determined by the voids and not so much by the properties of the material [6]. For a powder bed porosity of 50 % the conductivity of the powder bed is approx. 10x the conductivity of the gas in the powder bed. The inert gas used is argon which has a conductivity from 0.02 to 0.03 $Wm^{-1}K^{-1}$ increasing with temperature from room to solidus temperature (i.e. 293 to 1878 K) [11]. The conductivity of the powder is therefore modeled linearly increasing from 0.2 to 0.3 $Wm^{-1}K^{-1}$.

The influence of the powder bed porosity and the inert gas on the specific heat capacity of the powder bed is minute; therefore the nominal values are used. The powder bed density follows from the powder bed porosity of 50 %. The change in properties from powder to melt is triggered by a user variable implemented using the user subroutine USDFLD to ensure that powder melts to liquid, but solidifies to solid and not to powder.

2.3 Simulation results

To understand the global behavior of the numerical model, the melt pool shape, indicated in blue, is investigated at the extremes of the parameter ranges as shown in Figure 3. Vertically, the scan velocity is increased from 100 to 1525 mm/s and horizontally the laser power is increased from 40 to 400 W.

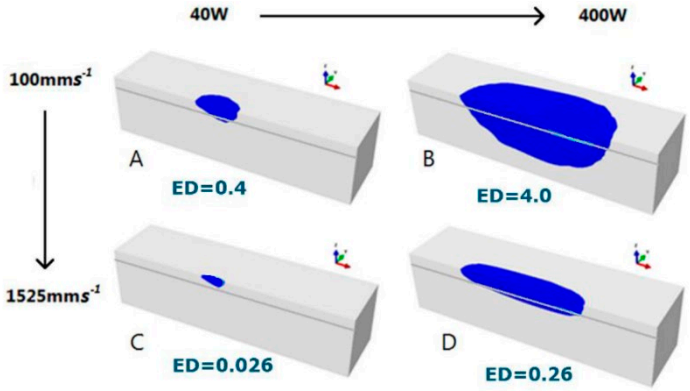

Figure 3. *Melt pool shape (in blue) at the extremes of the parameter ranges of the laser scan speed and the laser power.*

Cases A and D have similar energy densities. Hence, the melt pool width and depth are also similar. However, due to the higher scan speed the melt pool of Case D is much longer. Case B has the highest energy density and therefore also the biggest melt pool largely penetrating the modelled solid substrate (i.e. the previously deposited layer). In fact, from the figure it can be concluded that multiple previously deposited layers will be remelted. In most cases this is considered unwanted. Based on the results of the extremes of the parameter ranges of Figure 3, a more interesting energy density range was determined from 0.11 to 0.8 J/mm. In this work the energy density is formulated in the unit of J/mm, because the layer thickness and the spot size are constant for all simulations.
For proper attachment the melt pool should extend into the previously deposited layer. Figure 4 shows the melt pool shape for increasing energy density in the (remelted) layer only. Hence, compared to Figure 3 the upper powder bed layer of 100 µm is removed in the figures.

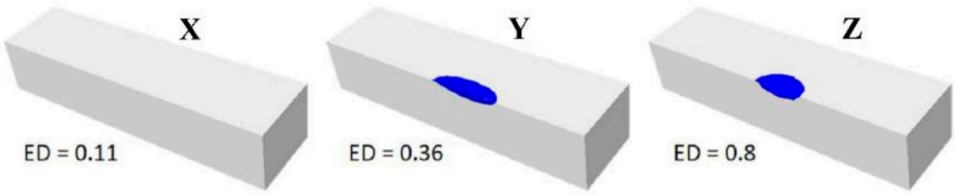

Figure 4. *Remelting of the previously deposited layer only, for increasing Energy Density (ED). The upper powder bed layer of 100 µm is removed in the figures.*

Figure 4 shows that the remelted zone depends strongly on the energy density. For Case X, with a relative low energy density, the energy density is too low to penetrate the powder bed layer and therefore no attachment is predicted. Case Y, in which the energy density is 0.36 J/mm, predicts the best results as the remelted zone approximately equals the vector width. For Case Z, with the highest energy density, the remelted zone is larger than the vector width.

3 Experimental validation – scan vector attachment

The numerical model is validated by selective laser melting an extensive number of vectors with varying process parameters. All experiments are conducted on an SLM Solutions SLM280HL machine with a 400 W laser. Ten-layer vectors with a platform lowering of 50 µm per layer are scanned with a 70 µm laser spot diameter leading to thin walls of material. These vectors are built on top of a platform that was created using SLM in the same build job. Due to the assumed porosity of the powder bed layer of 50 %, the actual powder bed thickness being scanned is twice the platform lowering (i.e. the modeled 100 µm powder bed thickness). This value is stable during the 10 layers because the platform was also made using SLM.
Samples of 30x30 mm were printed (see Figure 5), in which the laser power was varied from 40 to 400 W and the scan velocity was varied from 100 to 1525 mm/s according to the extremes in Figure 3. The assumption is made that the laser power and speed settings are actually realized by the machine. This was not validated separately for these experiments. According to chosen process window, the energy densities varied between 0.02 and 4.0 J/mm. Typical production settings indicate that the most interesting energy densities range from 0.2 to 0.36 J/mm. The variation of the laser process parameters is also illustrated in Figure 5.

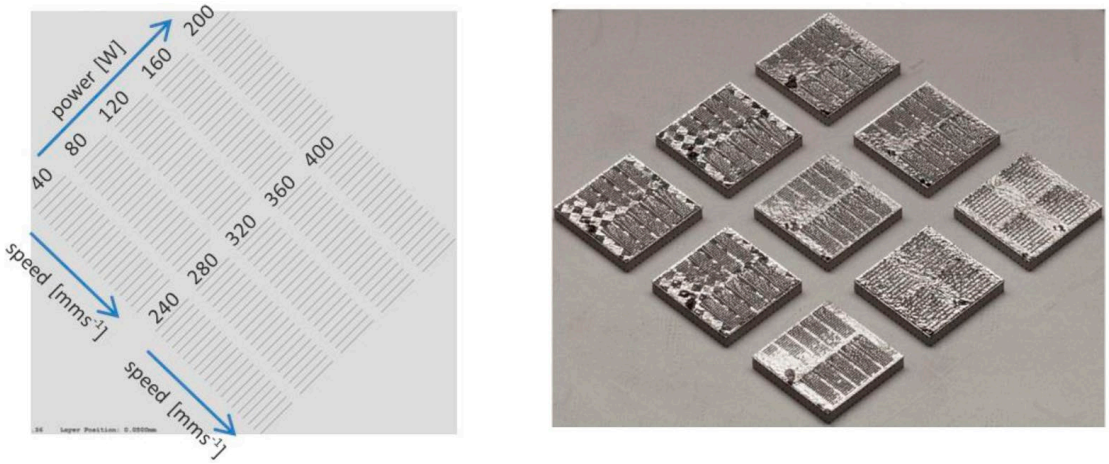

Figure 5. *Variation of laser process parameters (left) and a photograph of several printed samples (right).*

The produced samples are cut across and inspected through a microscope. Figure 6 shows the resulting cross-sections. The red, blue and green boxes indicate identical energy densities, but obtained with a different combination of process parameters. The yellow boxes indicate that process parameters are used that are the same as for the simulated results shown in Figure 3. Underneath each cross-section the energy density is also given. In general, in the top right area insufficient energy density is used. The wall is either not build at all or shows large porosities (the black areas in the figure correspond to no material presence in the cross-section). Contrary, in the lower left area too high energy density is used, leading to excessive melting and spilling, which leads to a very wide wall or even walls that interconnect. Also, increasing the laser power but maintaining a similar energy density, tends to lead to wider scan vectors. Note that the meaning of Figure 6 is to show the overall attachment performance for a wide range of energy densities. Local remelted material boundaries and microstructure formation are not considered here.

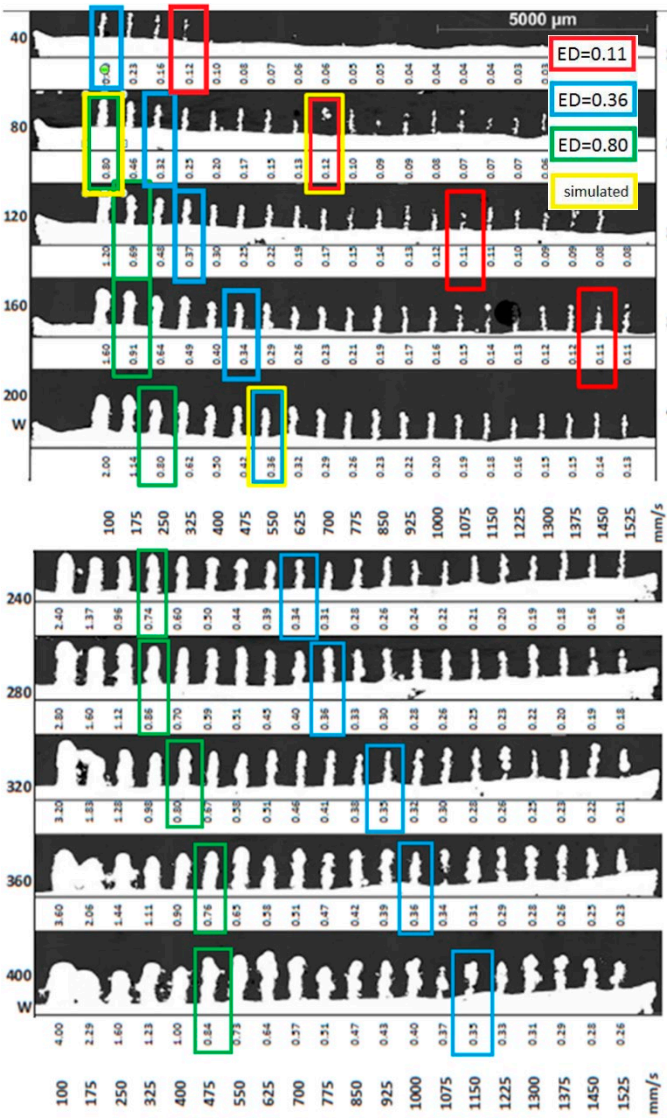

Figure 6. *Cross-section cuts of ten-layer single scan width vectors with laser power from 40 to 400 W and scan velocity from 100 to 1525 mm/s.*

The red boxes with an energy density of 0.11 J/mm clearly show that no proper attachment occurred, because there are large pores in the wall. Also, the simulations show no re-melting of the previously deposited material and therefore the simulation predict that no proper attachment will be formed. The blue and green boxes with energy densities of 0.36 J/mm and 0.8 J/mm, respectively, in general show no pores and therefore a fully dense product can be expected. For these energy densities the simulations show that part of the previously deposited material is indeed remelted and therefore the newly melted material will properly adhere to the already deposited material. It should be noted that in the experiments 9 of the 10 layers are built on top of a previous vector instead of on top of the initially built platform. The simulation places a single vector on a solid substrate of the same material; hence, modelling an ideal flat previously deposited layer. This does lead to differences in heat transfer behavior, which are subject of a future study.

4 Experimental validation – scan vector width

To check the capability of the numerical model to predict the actual geometry of the scan vectors (i.e. not only melt depth and attachment, but also track width) the scan vector widths are also analyzed. For this analysis, single layer vector experimental results are also used. These were made for different powder layer thicknesses. The single layer scan vector width was measured from a top image, whereas the ten-layer scan vector width was measured from a cross-section similar to those in Figure 6. Based on the ten-layer scan vector attachment results, the energy density was varied from 0.2 to 0.9 J/mm. For this experiment a platform lowering distance per layer of both 40 and 60 µm was used. As the results for these layer thicknesses were similar to the previous scan vector attachment experiment, the numerical simulations were only made for the 50 µm platform lowering distance (i.e. 100 µm modeled powder layer thickness).
Figure 7 shows a top view image of a printed sample for the single layer scan vector experiment. In this case the layer thickness was 40 µm and the laser power was 200W. The energy density was varied from 0.2 to 0.9 J/mm from left to right in the image and the scan direction was bottom to top. Also, a close-up magnification (10x) is shown on the right hand side. Typical weld-like shapes are visible on the top surface, including many small round particles in the periphery of the scan vector. The round particles are either spattering droplets due to the process or (partly) melted powder particles. The scan vector width was determined using Matlab's image processing toolbox.

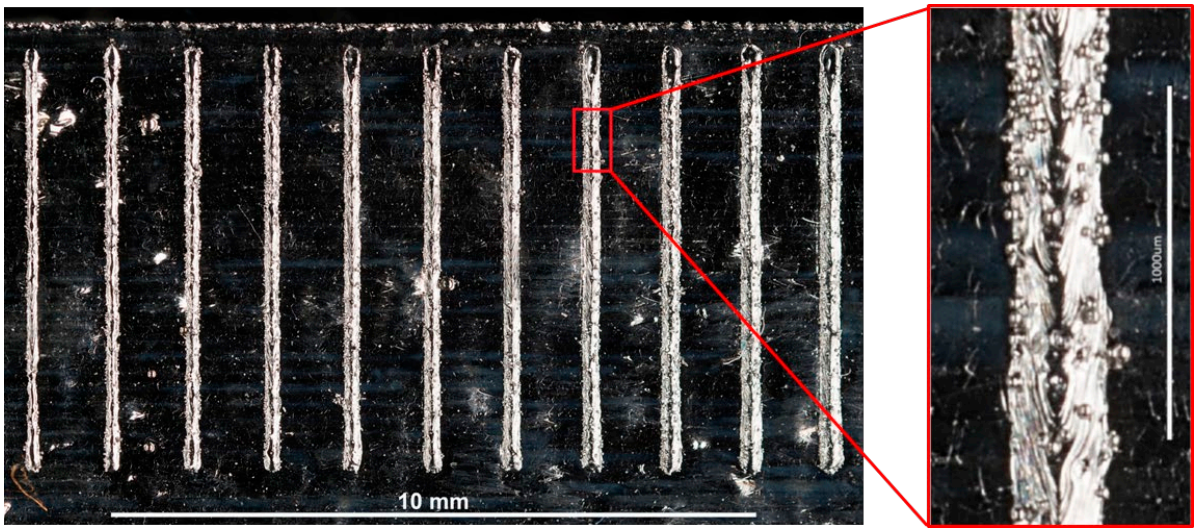

Figure 7. *Printed sample top view and close-up magnification (10x) to measure single scan vector widths for a layer thickness of 40 µm, a laser power of 200 W and a varied energy density from 0.2 to 0.9 J/mm (left to right).*

Figure 8 shows both the measured and simulated results for the extended experiment. The blue, red, green and pink dots indicate the scan vector width obtained from the experiment. The orange dots indicate the simulated scan vector widths. The single layer experiments were not executed for all laser powers based on the observation that the single layer widths match well with the ten-layer vectors. Also, due to the calculation time not all laser powers and energy densities were simulated.

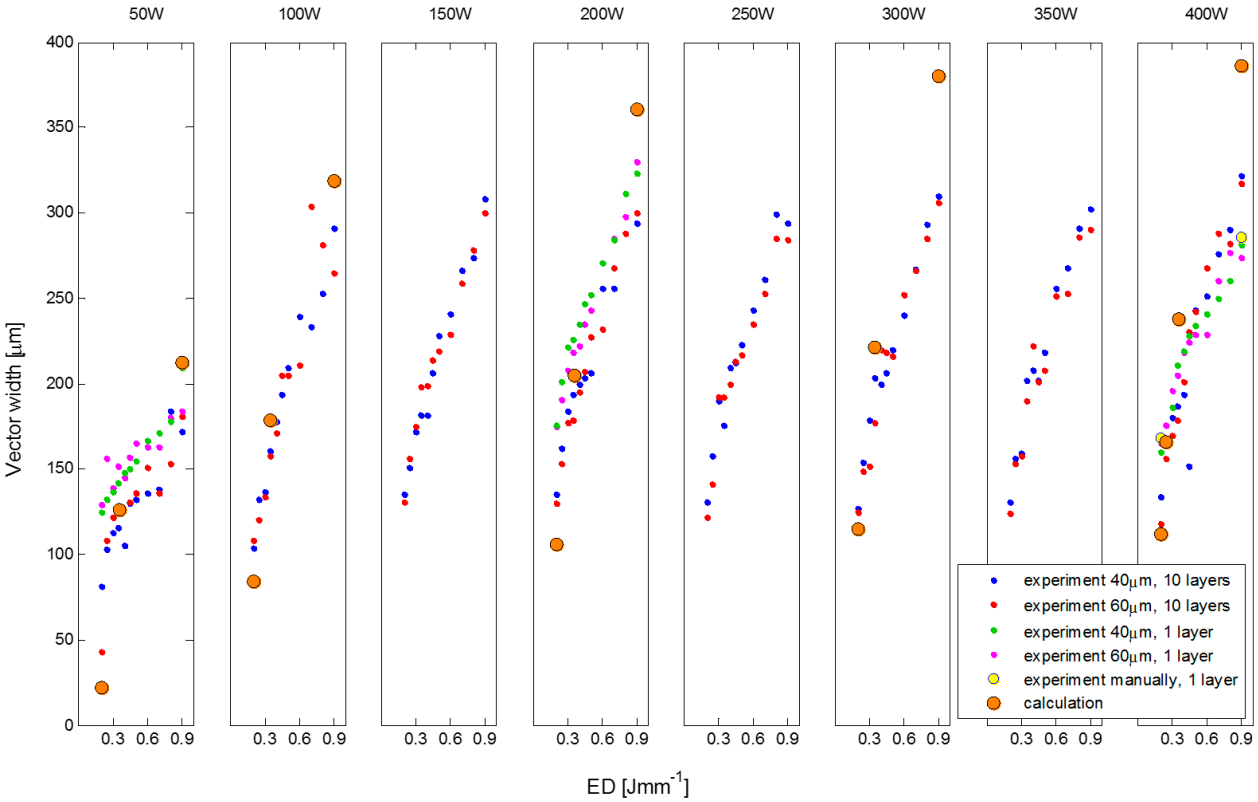

Figure 8. *Measured and simulated scan vector widths for laser powers from 50 to 400 W and energy densities from 0.2 to 0.9 J/mm.*

In general, the results from the simulations compare well with the experimental results. The simulated values follow the trend of the measured values. Also, the single layer and ten-layer experiments match well; although the single layer scan vector widths tend to be a bit wider. This deviation can be attributed to the different measurement surface (i.e. top image vs. cross-section image).
For low energy densities (i.e. ED = 0.2 J/mm) and laser powers below 300 W the vector width is slightly under predicted by about 10 % (20 µm). This is due to the fact that at such low energy densities and low laser powers the boundary of a stable process window is reached, as the drop in measured vector widths also indicate.
For medium energy densities (i.e. ED = 0.36 J/mm) the simulated and measured results match perfectly. Hence, for typical production settings, in which such energy densities are commonly used, the predicted vector widths are most accurate.
Finally, for high energy densities (i.e. ED = 0.9 J/mm) the results match well for laser powers up to 200 W. At 200 W, 300 W and 400 W the simulated vector width is over predicted by 16 %, 23 % and 29 %, respectively. In the model evaporation is neglected. Evaporation extracts energy from the melt pool and creates a laser absorbing vapor. This leads to a smaller vector width. Evaporation is expected to be higher for increased laser powers, since then energy is applied to the melt pool in the shortest time. The heat diffusion is lower and the temperature gradients are expected to be higher.
This assumption was validated by also implementing Langmuir's equation for evaporative mass rate in the model [12-13]. This lead to realistic melt pool temperatures in the order of 2400 K; however, the vector widths were then under predicted. The reason for this effect is that Langmuir's equation is valid for absolute vacuum conditions only; hence, this implementation can be regarded as the upper extreme case.

5 Conclusions

A numerical model is presented to predict single scan vectors in selective laser melting, taking into account the powder properties, scan speed, laser power absorption and heat conduction. The numerical model has been validated using measurement data obtained from vector scanning experiments using titanium alloy Ti6Al4V.
The numerical model can accurately predict vector widths for medium laser energy densities (~0.36 J/mm) as are commonly used in selective laser melting. For low energy densities (~0.2 J/mm) and laser powers below 300 W the model slightly under predicts the vector width by about 10%. For high energy densities (~0.9 J/mm) and laser powers larger than 200 W the model over predicts the vector width by about 25%, which is attributed to evaporation effects that were not included in the model.
Future work should incorporate a better evaporative energy term for the melt pool and laser absorption by the vapor. Also, different materials and powders should be validated.

6 References

[1] EU AM Platform, 2014, Additive manufacturing: Strategic research agenda.

[2] Shiomi, M., Osakada, K., Nakamura, K., Yamashita, T., Abe F., 2004, Residual stress within metallic model made by selective laser melting process, CIRP Annals - Manufacturing Technology, Vol. 53, No. 1, pp. 195-198.

[3] Yadroitsev, I., 2009, Selective laser melting - Direct manufacturing of 3D-objects by selective laser melting of metal powders. Lambert Academic Publishing.

[4] Kruth, J.-P., Levy, G., Klocke, F., Childs, T.H.C., 2007, Consolidation phenomena in laser and powder-bed based layered manufacturing, CIRP Annals - Manufacturing Technology, Vol. 56 (2).

[5] Yadroitsev, I., Smurov, I., 2010, Selective laser melting technology: from the single laser melted track stability to 3D parts of complex shape, Physics Procedia 5, pp. 551–560.

[6] Gusarov, A.V., Yadroitsev, I., Bertrand, Ph., Smurov, I., 2007, Heat transfer modelling and stability analysis of selective laser melting, Applied Surface Science 254, pp. 975–979.

[7] Chandrasekhar, S., Hydrodynamic and hydromagnetic stability, Clarendon Press, Oxford, 1961.

[8] Gusarov, A.V., Smurov, I., 2010, Modeling the interaction of laser radiation with powder bed at selective laser melting, Physics Procedia 5, pp. 381–394.

[9] Gusarov, A.V., Smurov, I., 2010, Radiation transfer in metallic powder beds used in laser processing, Journal of Quantitative Spectroscopy & Radiative Transfer 111 pp. 2517–2527.

[10] Mills, K., 2002, Recommended values of thermophysical properties for selected commercial alloys, Woodhead publishing limited.

[11] Younglove, B., Hanley, H., 1986, The viscosity and thermal conductivity coefficients of gaseous and liquid argon, Journal of Physical and Chemical Reference Data 15 (4), pp. 1323–1337.

[12] Verhaeghe, F., Craeghs, T., Heulens, J., Pandelaers, L., 2009, A pragmatic model for selective laser melting with evaporation. Acta Materiala 57, 6006–6012.

[13] Lei, Y.P., Murakawa, H., Shi, Y.W., Li, X.Y., 2001, Numerical analysis of the competitive influence of Marangoni flow and evaporation on heat surface temperature and molten pool shape in laser surface remelting, Computational Materials Science, Vol. 21 (3), pp 276-290.

NLR

Anthony Fokkerweg 2

1059 CM Amsterdam

p) +31 88 511 3113 f) +31 88 511 3210

e) info@nlr.nl i) www.nlr.nl